This is the peer reviewd version of the followng article:

Polychromatic emission in a wide energy range from InP-InAs-InP multi-shell nanowires / Battiato, S.; Wu, S.; Zannier, V.; Bertoni, A.; Goldoni, G.; Li, A.; Xiao, S.; Han, X. D.; Beltram, F.; Sorba, L.; Xu, X.; Rossella, F.. - In: NANOTECHNOLOGY. - ISSN 1361-6528. - 30:19(2019), pp. 1-9. [10.1088/1361-6528/aafde4]

Terms of use:

The terms and conditions for the reuse of this version of the manuscript are specified in the publishing policy. For all terms of use and more information see the publisher's website.

03/05/2026 13:11

(Article begins on next page)

Nanotechnology

ACCEPTED MANUSCRIPT

Polychromatic emission in a wide energy range from InP-InAs-InP multi-shell nanowires

To cite this article before publication: Sergio Battiato *et al* 2019 *Nanotechnology* in press https://doi.org/10.1088/1361-6528/aafde4

Manuscript version: Accepted Manuscript

Accepted Manuscript is “the version of the article accepted for publication including all changes made as a result of the peer review process, and which may also include the addition to the article by IOP Publishing of a header, an article ID, a cover sheet and/or an ‘Accepted Manuscript’ watermark, but excluding any other editing, typesetting or other changes made by IOP Publishing and/or its licensors”

This Accepted Manuscript is **© 2019 IOP Publishing Ltd**.

During the embargo period (the 12 month period from the publication of the Version of Record of this article), the Accepted Manuscript is fully protected by copyright and cannot be reused or reposted elsewhere.
As the Version of Record of this article is going to be / has been published on a subscription basis, this Accepted Manuscript is available for reuse under a CC BY-NC-ND 3.0 licence after the 12 month embargo period.

After the embargo period, everyone is permitted to use copy and redistribute this article for non-commercial purposes only, provided that they adhere to all the terms of the licence https://creativecommons.org/licences/by-nc-nd/3.0

Although reasonable endeavours have been taken to obtain all necessary permissions from third parties to include their copyrighted content within this article, their full citation and copyright line may not be present in this Accepted Manuscript version. Before using any content from this article, please refer to the Version of Record on IOPscience once published for full citation and copyright details, as permissions will likely be required. All third party content is fully copyright protected, unless specifically stated otherwise in the figure caption in the Version of Record.

View the article online for updates and enhancements.

This content was downloaded from IP address 129.186.138.35 on 15/01/2019 at 18:20

IOP Publishing Journal Title
Journal **XX** (XXXX) XXXXXX https://doi.org/XXXX/XXXX

Polychromatic emission in a wide energy range from InP-InAs-InP multi-shell nanowires

S. Battiato[1,¶], S. Wu[2,¶], V. Zannier[1], A. Bertoni[3], G. Goldoni[3,4], A. Li[5], S. Xiao[2], X. D. Han[5], F. Beltram[1], L. Sorba[1], X. Xu[2,6,7], F. Rossella[1]

[1] NEST, Scuola Normale Superiore and Istituto Nanoscienze-CNR, 56217 Pisa, Italy
[2] Beijing National Laboratory for Condensed Matter Physics, Institute of Physics, Chinese Academy of Science, Beijing 100190, China
[3] S3, Istituto Nanoscienze-CNR, 41125 Modena, Italy
[4] Dipartimento di Fisica, Informatica e Matematica, Università di Modena e Reggio Emilia, Italy
[5] Beijing Key Laboratory of Microstructure and Properties of Solids, Beijing University of Technology, Pingleyuan No.100, 100124, Beijing, P. R. China
[6] CAS Center for Excellence in Topological Quantum Computation and School of Physical Sciences, University of Chinese Academy of Sciences, Beijing 100049, China
[7] Songshan Lake Materials Laboratory, Dongguan, Guangdong 523808, China
[¶] contributed equally to this work

E-mail: Francesco.rossella@sns.it

Received xxxxxx
Accepted for publication xxxxxx
Published xxxxxx

Abstract

InP-InAs-InP multi-shell nanowires (NWs) were grown in the wurtzite or zincblende crystal phase and their photoluminescence (PL) properties were investigated at low temperature (≈6K) for different measurement geometries. PL emissions from the NWs were carefully studied in a wide energy range from 0.7 eV to 1.6 eV. The different features observed in the PL spectra for increasing energies are attributed to four distinct emitting domains of these nano-heterostructures: the InAs island (axially grown), the thin InAs capping shell (radially grown), the crystal-phase quantum disks arising from the coexistence of InP zincblende and wurtzite segments in the same NW, and the InP portions of the NW.
These results provide a useful frame for the rational implementation of InP-InAs-InP multi-shell NWs containing various quantum confined domains as polychromatic optically active components in nanodevices for quantum information and communication technologies.

Keywords: InP-InAs-InP heterostructure, multi-shell nanowire, photoluminescence

1. Introduction

The shape, the dimensions and the ease of combining different semiconductor materials peculiar of nanowires (NWs), make these nanostructures ideal candidates as building blocks for the implementation of novel devices [1]. Even novel materials become available in this context. For instance the lattice structure of non-nitride III-V NWs is wurtzite (WZ), a crystal phase that can not be found in the bulk where the zincblende (ZB) structure is instead ubiquitous in these materials [2]. Growth techniques yield a high degree of control particularly on InAs and InP semiconductor materials, and experimental and theoretical investigations on high-quality samples have made it possible to investigate all relevant structural, electronic and optical properties [3,4,5]. Another degree of freedom stems from the possibility to combine axially in the same NW InAs and InP

 © xxxx IOP Publishing Ltd

Accepted Manuscript

semiconductors [6,7]. This has opened a new window of application of NWs in quantum devices, with the manipulation of single degrees of freedom of individual electrons or photons: a key ingredient for spintronics and quantum information and communication technologies [8,9]. This was demonstrated for transport devices typically resorting to thin InP barriers to confine electrons in an InAs island [10,11,12], while for optical devices usually single photon manipulation is achieved exploiting the technology of InAsP quantum dots emitting in the energy range from 1.3 eV to 1.41 eV [13,14,15].

An exciting development of the InAs-InP NW technology is represented by the InP-InAs-InP multi-shell NWs [16-20]. These consist of an InP stem surrounded by a thin InAs shell with an axial InAs island and capped with a thick InP outer shell. The thickness of the InAs shell around the InP NW can be finely tuned and the shell can be regarded as a strained InAs quantum well (QW). The optical properties of these systems have been investigated using photoluminescence (PL) with PL bands centered at energies ranging from 1.3 eV to 0.8 eV for a InAs QW thickness in the range from two monolayers (MLs) up to more than ten MLs. Usually the investigations focus on the energy window characteristic of the PL attributed to a specific InAs well thickness, thus only a small portion of the full PL spectrum that is characteristic of the entire NW system under probe is measured. Additionally, PL studies were frequently probing an ensemble of NWs rather than an individual InP-InAs-InP multi-shell NW systems. The comprehensive investigation of the full PL properties of InP-InAs-InP multi-shell NWs and their correlation to the crystal structure is however unreported.

In fact, due to the structure complexity of the emitting system, the pristine PL spectra display bands in a wide energy range, spanning from a minimum energy value set by the energy characteristic of the large InAs island (formed on the top of the InP stem due to the axial growth), to a maximum value set by the InP portions of the NW. The energy values of the reported PL features are much influenced by key parameters such as the crystal phase, the strained InAs bandgap, the exact dimension of each individual nano-emitter composing the NW (InP stem, InAs well and island, and InP shell), and last but not least the defects present in the NW system. In particular, emitters due to the coexistence of ZB and WZ segments present in the same NW can be observed in the PL spectra. In fact, confinement due to the band offset between the two phases yields to a low dimensional system, referred to as a crystal-phase quantum disk, that is optically active in an energy region slightly red-shifted with respect to the PL from the InP stem [21].

In this work, by means of Au-assisted Chemical Beam Epitaxy (CBE) [22], we have grown InP-InAs-InP multi-shell NWs consisting of an InP stem with a diameter of 30 nm, surrounded by a few ML-thick InAs well with an axial InAs island, and capped with a 15 nm-thick InP outer shell. NWs were grown both in the pure ZB or mixed ZB/WZ crystal phases by properly choosing the substrate orientation. We investigated the PL properties of our samples at low temperature (≈ 6 K) using different measurement geometries, i.e. shining the laser probe onto ensembles of vertical NWs self-standing on the InP growth substrate, and onto individual NWs drop casted onto a SiO_2 substrate. All the PL peaks in the energy range from 0.7 eV to 1.6 eV were characterized in the same NW sample. The sequence of the observed PL peaks was attributed to (i) the InAs island, (ii) the few ML InAs quantum well, (iii) the crystal-phase quantum disks due to the coexistence of InP ZB and WZ segments in the same NW, and (iv) the InP portions of the NW. These PL features are observed at increasing energies from (i) to (iv), and the occurrence and the characteristics of the peaks are correlated to the dominant character of the crystal phase of the NWs. Numerical simulations of the electron and hole wavefunctions in different cross sectional areas of the NWs were performed: the resulting calculated emission energies from the island and QW of InAs are in good agreement with experiments. We believe the present results can be of much use for the exploitation of InP-InAs-InP multi-shell NWs as polychromatic optical active components in nanodevices for quantum information and communication technologies.

2. Methods

A schematic representation of the InP-InAs-InP multi-shell NWs presented in this paper is reported in figure 1, where we illustrate the structure of the system: (i) InP NW stem, (ii) InAs shell and axial island, (iii) InP outer shell and top segment. The multi-shell NWs of the present study were grown by Au-assisted CBE in a Riber Compact-21 system. We used InP(111)B and InP(100)-oriented substrates. The growth was initiated by using gold colloids as catalyst, following the Au-assisted VLS mechanism. Monodispersed Au particles of 20 nm in diameter were obtained by drop casting of the colloidal solution. The substrate temperature was set at 390°C ± 10°C, trimethylindium (TMIn), tert-butylarsine (TBAs) and tert-butylphosphine (TBP) were used as metalorganic sources of indium, arsenic and phosphorus, respectively. TBAs and TBP precursors were pre-cracked in a high temperature injector kept at 1000 °C since the substrate temperature is not sufficient for their decomposition, while TMIn requires a lower decomposition temperature and decomposes directly at the substrate surface. Precursor fluxes were controlled by regulating the metalorganic line pressures through needle valves. The growth of the InP NW stem and outer shell was performed

Accepted Manuscript

on both substrate orientations using line pressures of 0.3 and 0.77 Torr for TMIn and TBP, respectively. The InAs growth was performed at the same substrate temperature, using the same TMIn line pressure (0.3 Torr), but different TBAs line pressures for the growth on two different substrates: 1.5 Torr for InP(100) and 0.77 Torr for InP(111)B substrate. These conditions ensure the growth of straight and vertically-oriented multi-shell NWs on both substrates. All the samples were cooled down in UHV environment, after simultaneously switching off both group III and V precursor fluxes.

The NWs morphology was characterized using a Zeiss field-emission Scanning Electron Microscopy (SEM) operated at 5 kV. The structure analysis of the NWs was performed by employing a probe aberration-corrected transmission electron microscopy (TEM) Titan Themis (Thermo Fisher Scientific) which was equipped with a monochrometer and Super EDS detector and operated at 300 kV.

PL studies were performed as function of the incident laser power and polarization and for different measurement configuration geometry: (a) ensemble of vertical self-standing NWs onto the pristine InP substrate, or (b) individual NWs drop casted onto a SiO_2 substrate. The sample chip was placed on a xyz-piezoelectric stage in the cryostat at 4.2 K. The measurement configurations used in this work are schematically depicted in figure 2, top, while the setup for micro-PL measurement is shown in figure 2, bottom. We performed micro-PL measurements using a confocal microscopy furnished with a numerical aperture of NA = 0.75 microscope objective. A complementary metal oxide semiconductor (CMOS) camera was equipped to identify the orientation and position of the NW. Non-resonant excitation was carried out by a 532 nm laser for PL measurements. The PL of NWs was collected and dispersed via a 0.55 m spectrometer, and the signal was detected with a liquid cooled charge coupled device camera (CCD) and InGaAs camera with a spectra resolution of 60 μeV. The half-wave plate polarizer were added in the collection path to measure the polarized PL spectra.

Numerical simulations of electron and hole states confined in the QW have been performed by assuming translational invariance along the nanowire axis. We calculated electron states in the envelope function approximation assuming parabolic bands and a hexagonal section. The computational approach employs a finite-volume integration algorithm with a grid of 57500 nodes. We used a hexagonal tessellation of the hexagonal domain [23,24]. This choice proved to be necessary in order to reproduce the proper degeneracies in the energy spectra. Effective mass values and band gaps of the nanowire materials were $m_e^* = 0.023\ m_e$ and $m_h^* = 0.41\ m_e$ for InAs, $m_e^* = 0.08\ m_e$ and $m_h^* = 0.6\ m_e$ for InP; E_g = 0.515 eV for strained InAs [25,26,27] (see section 3.3), E_g = 1.42 eV for InP.

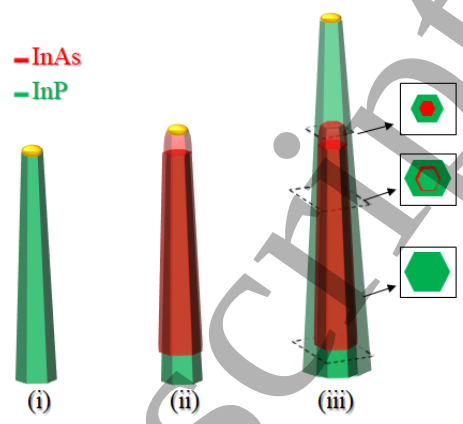

Figure 1 Schematic of an InP-InAs-InP multi-shell NW, illustrating the different structure components of the nanostructure: (i) the InP stem, (ii) the InAs island and shell, (iii) the InP top segment and outer shell.

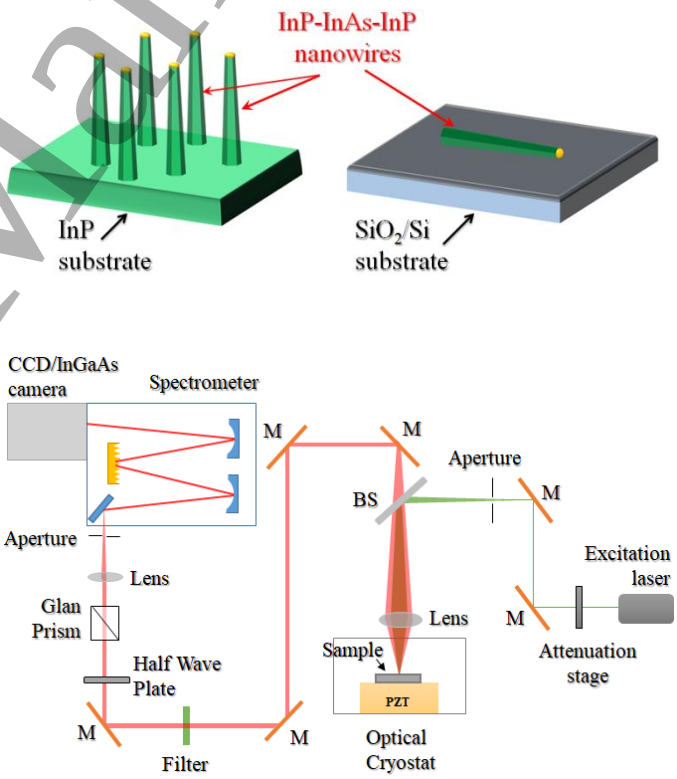

Figure 2 (Top) Multi-shell nanowire samples used in this work: (left) ensemble of vertical nanowires self-standing on the InP substrate; (right) single nanowire drop casted onto a SiO_2/Si substrate. (Bottom) Schematic diagram of the setup for micro-photoluminescence used for the measurements of ensemble of vertical nanowires and of individual nanowires.

Accepted Manuscript

3. Results

3.1 Morphological and structural analysis

Figure 3 reports SEM micrographs of our NW samples at different stages of the growth process. The InP stems grown on InP(111)B and (100) substrates (figure 3a,b) are vertically standing and grow along the <111> and <100> direction, respectively. The insets highlight the square or hexagonal shape of (100) or (111)B oriented InP NWs, respectively. SEM images of the multi-shell NW nanostructures are reported in figure 3c, d. Here, the increased diameter and length of the nanostructures account for the presence of the buried InAs island and radial QW, terminated with the InP top segment and surrounded by the thick InP outer shell. We notice our nanowires display tapering, that we ascribe to the low temperature conditions during the growth. The study of the possible correlation between this morphological feature and the PL features - technically quite challenging - goes beyond the purpose of the present work and will be the object of future investigations.

From the high resolution STEM analysis (see figure 4) we found that NWs grown on InP(100) have pure ZB crystal structure, while NWs grown on InP(111)B have a mixed ZB/WZ crystal structure. This is well visible in panels(b) and (d) of figure 4, where we show high resolution HAADF-STEM images with the correspondent selected area electron diffraction (SAED) patterns of a small NW portion containing the InAs island taken along [110] zone axis. The Z-contrast between the two different semiconductor materials returns information on the actual structure of the multi-shell NWs, on the interfaces between the two materials, and on the dimension of the quantum confined structures. Actually, the different crystal structure arises from the different growth axis of the NWs which are the <100> and the <111>B directions on the (100) and (111)B InP substrates, respectively. Indeed, the energetic differences for hexagonal or cubic stacking sequences in the <111> direction are very small [28]. As a consequence stacking faults easily occur in InP NWs vertically grown on <111>B oriented substrates, giving nanowires with alternating WZ/ZB segments. On the other hand, the formation of similar defects during growth in the <100> direction needs to overcome an activation barrier, while the cubic stacking sequence without the formation of defect is stable. That's why defect-free ZB InP NWs are obtained on (100) oriented substrates.

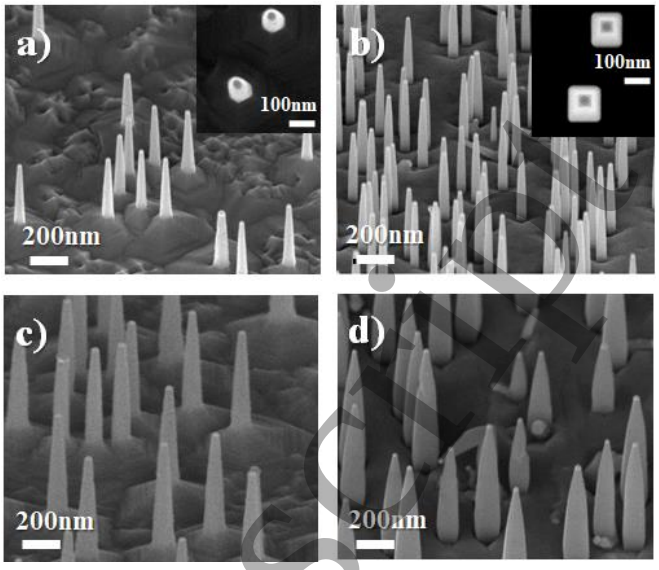

Figure 3 SEM micrographs (45° tilted) of NW samples at different growth stages: InP stems (a, b) and InP-InAs-InP multi-shell NWs (c, d) The NW samples were grown on InP (111)B (a, c) and on InP (100) (b, d) substrates. Insets in panels (a) and (b) represent the corresponding top-view micrographs.

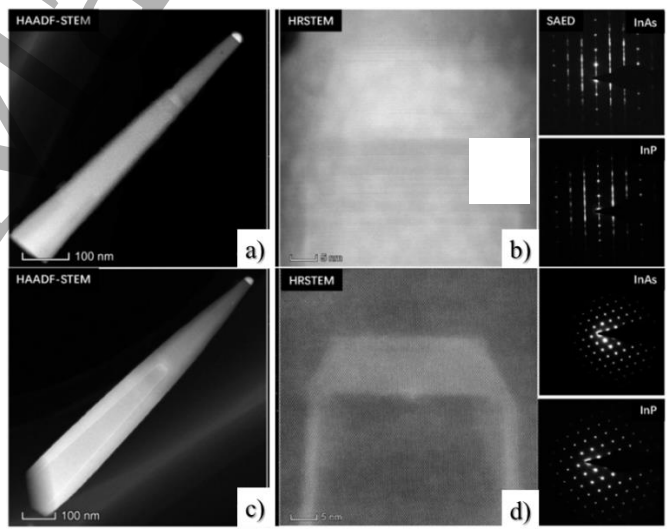

Figure 4 High resolution STEM micrographs of individual InAs-InP multi shell NWs with mixed ZB/WZ (a, b) or pure ZB (c, d) crystal phase, and their corresponding selected area electron diffraction patterns (ZA [110]). In the NWs grown on InP(111)B the ZB and WZ crystal phases coexist, yielding to a band-offset that may induce confinement in the axial direction.

According to HRTEM and EDS analysis (see Supplementary data), the InAs island, InAs QW, and the InP shell exhibit sharp interfaces. The InAs island is typically 30 nm wide and

Accepted Manuscript

8-10 nm high, while the InAs QW thickness is in the 2-8 ML range (≈ 0.7 nm – 3 nm). Moreover, the EDS analysis allowed us to conclude that both the island and the QW are made of pure InAs, i.e., there is no occurrence of interdiffusion of P. This is an important result in view of the PL study of our systems, since an intermixing of the group-V elements, affecting composition, strain and band alignment of the quantum structures, would very likely be detrimental to the PL features.

In our PL experiments, we probed the radiative recombinations of electron-hole pairs excited by the laser impinging on the nanowires. As far as concerns the emission from the InP sections of the nanowires, the ZB or mixed WZ/ZB character of the InP semiconductor can be likely reflected in a non-dramatic shift of the emission energy [4]. Regarding the emission from the WZ/ZB crystal phase quantum dots: the conduction and valence band offset between two adjacent InP segments with different phases generate a type II (staggered) heterojunction, which has an impact on the shape and spatial extension of the electron and hole wavefunctions, ultimately affecting the dynamics of electrons, holes and/or electron-hole pairs localized at the segments. This picture follows the scenario indicated by previous reports (e.g. reference [21] and in references therein) for what concerns the numerical value of the band offset between the ZB and WZ InP segments, i.e.: the WZ InP band gap exceeds the ZB InP one by ≈85 meV, and the WZ/ZB InP heterojunction has type II band alignment with the CB of WZ ≈130 meV above the CB of ZB, while the VB of WZ is ≈ 45 meV above the VB of ZB.

3.2 Photoluminescence from InAs-InP multi-shell NW samples

Figure 5 reports the PL spectra measured at temperature T≈6K, with excitation laser wavelength at 532 nm (laser spot size ≈2 μm) and power in the range 1-100 μeV, for different combinations of the multi-shell NW samples (ZB or mixed ZB/WZ crystal phase) and geometries (vertical NW ensemble or horizontal single NW). In all the spectra, we observed different bands corresponding to all the differently confined structures occurring in our NWs. Let us first examine the PL response of an ensemble of vertical multi-shell NWs. The excitation power-dependence of the PL spectra collected from the ZB or mixed ZB/WZ samples are reported in figure 5a and 5b, respectively. The shown energy window encompasses the energy characteristic of PL bands from the InP semiconductor material. The two main PL features occurring at ≈ 1.38 eV and 1.41 eV can be attributed to the bulk substrate and to the InP portions of the NWs, respectively, with different relative intensities likely reflecting the difference in the local density of NWs (number of NWs per um^2) probed by the laser spot [29]. The relatively broad distribution of the NW diameters in our samples can be grasped from the SEM images reported in figure 3 and is reflected in the occurrence of unavoidable differences in the energy position of the main PL band, resulting in a significant broadening, due to the simultaneous collection of the PL spectra from a number of NWs typically of the order of 100 for a laser spot of approximately 1-2 um^2.

The PL spectra from a single NW are reported in figures 5c and 5d and were measured in the energy range from 0.45 eV to 1.55 eV in order to address all the relevant PL features displayed in our multi-shell NW samples. For each panel we show the spectra of three different NWs, for comparison and for giving an idea of the fluctuation occurring in the PL features from NW to NW of the same as-grown sample. In the ZB sample (panel c), at the lowest energy side of the spectra we observed a band centered at ≈ 0.8 eV that we attribute to the ≈8 nm thick (typically 30 nm diameter) InAs island present at the top side of the thin (order of 1 nm) InAs shell. Similar PL bands were reported in references [17] and [20]. As it will be shown later in section 3.3, these spectra are fully consistent with the results of our numerical simulations performed assuming an InAs strained bandgap of 0.58 eV and considering an island 8 nm high and with a hexagonal section with diameter of ≈30-35 nm. At the high energy side of the spectra we find the PL peak from the InP body of the nanostructure, centered at ≈ 1.4 eV [3,4]. Between these two PL bands and in the energy range from 0.95 eV to 1.2 eV, we observed PL peaks whose precise energy may vary slightly in different individual NWs and may even depend on the exact position of the light probe along the same NW. Following [30, 20] and according to the results of our simulations (see section 3.3), we attribute the occurrence of these peaks to the presence of the radial shell (QW) of few MLs of ZB InAs.

PL spectra from three single NWs with mixed ZB/WZ crystal phase are reported in Fig. 5d. Here, the PL bands observed in the energy range from 0.9 eV to 1.1 eV can be attributed to the InAs structures - island and shell - and may sizably vary from NW to NW, due to differences in the NW diameter and InAs QW and island thickness. A PL peak centered at ≈ 1.42 eV was present in all measured NWs and is ascribed to the InP NW. Noticeably, in these samples, relatively narrow PL peaks are frequently observed in the energy range from 1.30 eV to 1.38 eV, that is, at energies lower respect to the PL from the InP NW but higher than the highest energy peak attributed to the InAs QW (≈ 1.2 eV). In this energy range, sharp and narrow PL peaks similar to those observed in our samples have been reported by Akopian and coworkers [21] in their PL study of chemically homogeneous InP NWs characterized by controlled sequences of axial sections with ZB or WZ crystal phase.

Accepted Manuscript

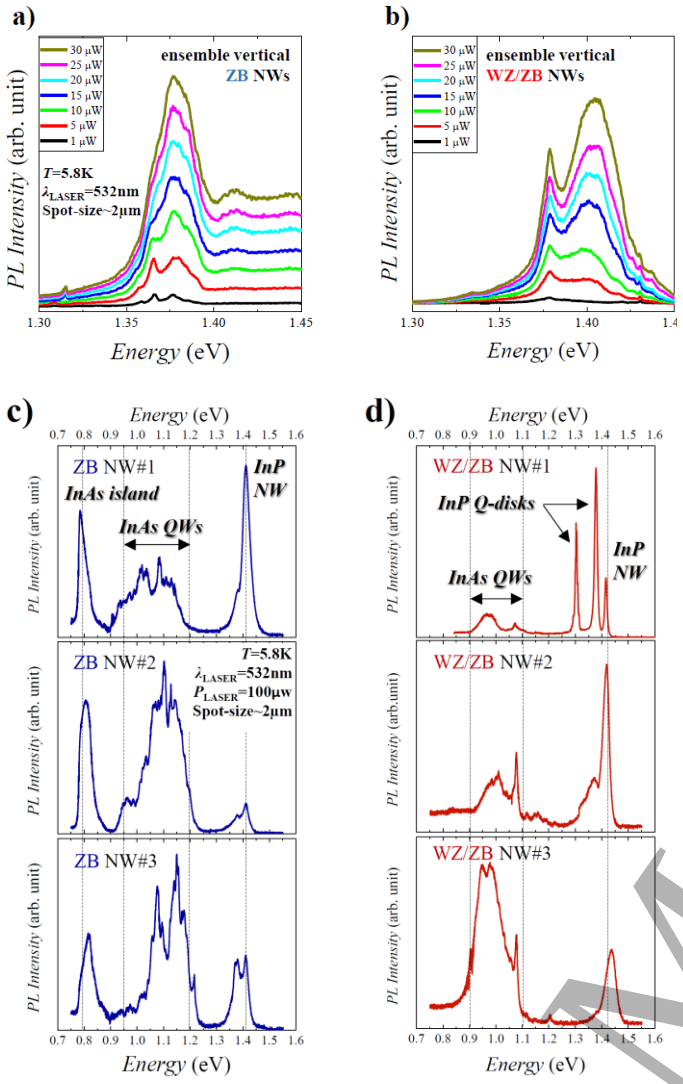

Figure 5 Photoluminescence spectra from InP-InAs-InP NW samples with different crystal phases, measured in different configurations: (a) ensemble of vertically oriented pure ZB and (b) mixed ZB/WZ NWs measured at different laser power, as indicated in the labels; (c) three individual pure ZB and (d) mixed ZB/WZ NWs drop casted onto a SiO_2/Si substrate.

As mentioned above the band-structure difference between the two phases can lead to charge confinement, thus enabling the engineering of the electronic structure in the absence of a change in chemical composition (crystal-phase quantum disks or quantum dots [21,31,32]). This type of carrier confinement can indeed represent an additional useful degree of freedom in device design at the nanoscale e.g. to implement single photon emitters, hence its relevance for advanced photonic applications in the frame of quantum information and communication technologies. For this reason, we decided to perform a more accurate analysis of these PL emissions. In the following section 3.4 we report the results of our study. Finally it is worth noting that, unfortunately, the room temperature emission from our nanowires does not conserve the characteristics displayed at 6 K (see Supporting Information). On the contrary, thermal broadening has severe impact on the emission features, smearing out and erasing the effects of quantum confinement.

3.3 Numerical simulations of the InAs QW and island

Figure 6 shows our modelling of the effect of quantum confinement of InAs on the PL emission energies, consistently with the occurrence of a type I (straggling gap) heterojunction at the interface between the InAs and InP semiconductors. This picture is invoked in most of the literature reporting experimental PL spectra from nanowire systems similar to the one investigated in this work (see for instance references [16, 20, 30] and references therein). We computed electron and hole states in an InAs QW of different thicknesses, wrapped around a InP stem with an hexagonal cross section and a diameter of 30 nm, and overgrown with a 15 nm-thick InP capping layer. Moreover, we performed the same simulations by substituting the core material with InAs in order to model the InAs island. While for the case of the InAs QW we suppose translational symmetry along the nanowire axis, we consider a height of 8 nm for the InAs island case. This value was chosen by inspecting TEM images of several samples.

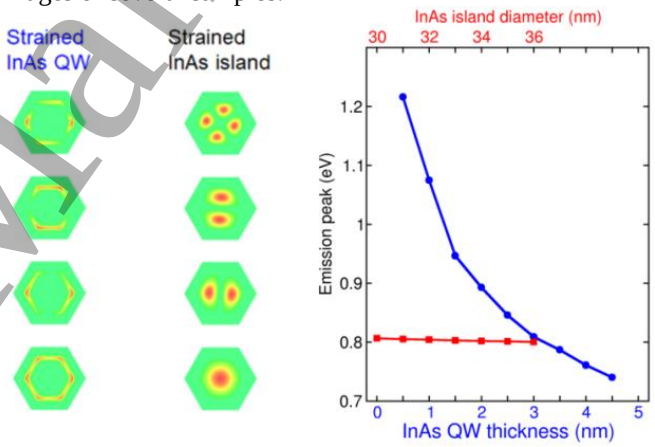

Figure 6 Left: Square modulus (probability distribution) in the nanowire cross-section of the electronic envelope functions of the four lower states (from bottom to top in increasing energy order) confined in a 2 nm thick InAs strained QW and in a 30 nm wide InAs island. Right: Numerical estimation of the PL peak energy from the hexagonal InAs QW (blue dots, bottom axis) and the InAs island (red squares, top axis) as a function of the QW thickness and island diameter, respectively.

Our results do not include excitonic binding energy [33], thus our estimated emission peaks are the sum of the confinement energy for the two carriers and the InAs energy gap. The choice of a reliable value for the latter energy is crucial. As indicated in section Methods, we used the low-temperature bulk InAs gap Eg = 0.415 eV [27] incremented

Accepted Manuscript

artificially by 0.1 eV due to the strain affecting the InAs material grown on InP. This increment, giving the experimental position of the island emission, is ~10% larger than the strain calculated for InP-InAs core-shell nanowires [24]. This is consistent with the fact that our thin InAs shell is embedded in InP material, rather than being the material core as in Ref. [4]. While the emission peak of the InAs island (≈0.8 eV) is essentially insensitive to its lateral dimension, the emission of the hexagonal QW is strongly dependent on the layer thickness. In the samples used for the present experiments, the QW has a thickness of 2 - 8 MLs, corresponding to about 0.7 - 3 nm. The computed emission range (0.8-1.2 eV) agrees well with the large band ascribed to the QW in figure 5c and 5d. We note that, although the QW thickness has a remarkable influence on the PL energy, for very thin layers a relevant part of the electron probability is localized in the core region. This is evident in the illustrative panels reporting the electronic envelope functions on the NW section, i.e. the square modulus of the first four electronic states confined in a 2 nm shell and in a 30 nm wide island.

3.4 Power- and polarization- dependence of the PL peaks from crystal-phase quantum disks

Figure 7 reports experimental results of our study of the PL from the InP crystal-phase quantum disks as function of the incident laser power and as a function of polarization. The power-dependent PL spectra reveal the occurrence of emission from the exciton (X0) and the biexciton (XX) of the WZ/ZB crystal-phase quantum disk in the InP NW body (see figure 7a). At relatively low excitation power (e.g. at 15 μW, or power density of ≈1μW/μm^2) the excitonic peak at about 1.299992 eV (955.663 nm) is recorded; by increasing excitation power its intensity increases. For an excitation power larger than 20 μW, the biexcitonic peak at 1.299905 eV (956.843 nm) appears in the PL spectra (its intensity increases with the excitation power), while the X0 peak intensity saturates. The presence of the two excitonic features in the PL spectra is exploited for the measurement of the fine structure splitting (FSS) that originates via the exchange interaction from asymmetries in the QD confinement potential.

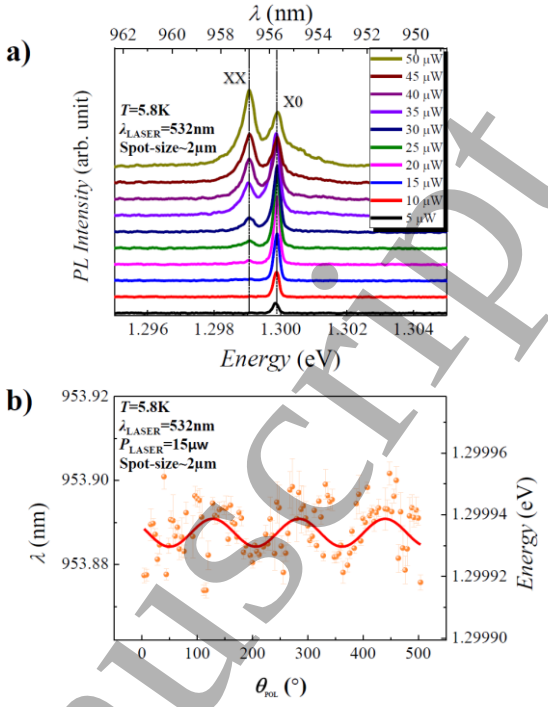

Figure 7 (a) PL emissions from InP crystal-phase quantum disks in a single nanowire, measured as a function of the excitation laser light power. (b) Energy of the X0 PL peak observed at low laser power, reported as a function of the light polarization degree, allowing the extraction of the fine structure splitting for this quantum confined system.

In general, the manipulation of the FSS in semiconductor quantum dots [34] is a key ingredient for quantum information [35] applications, since the radiative decay of excitonons/biexcitons could generate entangled photon pairs provided that a vanishing FSS is achieved [35,36]. Here we determined the FSS by means of polarization-dependent PL measurements, monitoring the modulation of the position (energy or wavelength) of the PL excitonic peak as function of the polarization angle, θ. In the present case we probed the FSS associated only with the X0 peak, due to the strong widening of the XX band at high excitation power. The polarization angle-dependence of the energy positions of the X0 peak measured in one of our NWs is reported in figure 7b and results in a FSS of approximately +10 μeV: this is caused by electron-hole exchange interaction and structure asymmetry of the WZ/ZB crystal-phase disks [37,38]. Typically, the sinusoidal fit to similar datasets with their error bars provide values of the FSS in the range 5-10 ueV (see Supporting Information). Typically, the sinusoidal fit to similar datasets with their error bars provide values of the FSS in the range 5-10 ueV (see Supporting Information). To reckon the relevance of this result, we have to consider that (i) for the generation of entangled photons, a vanishing FSS is targeted, and (ii) the value of the FSS typically reported for self-assembled quantum dot systems is in the range from 20

Accepted Manuscript

μeV to 100 μeV and beyond: we conclude that our system – displaying a FSS of 5-10 μeV - can be considered a quite promising candidate for the implementation of entangled photon sources [39].

4. Summary

In conclusion, we have grown InP-InAs-InP multi-shell NWs consisting of an InP NW stem with a diameter of 30 nm, surrounded by a few monolayer-thick InAs shell terminated with an axially grown InAs island, all capped with a 15 nm thick InP outer shell and axial top segment. The NWs were grown either in the pure ZB or in a mixed WZ/ZB crystal phase. We investigated the PL properties of our samples at temperature $T \approx 6$ K, both of ensembles of and individual NWs. The PL emission peaks observed were assigned to all the quantum confined emitters present in our NWs. PL bands at increasing energies were attributed respectively to (i) the InAs island, (ii) the few monolayer thick InAs shell, (iii) the crystal-phase quantum disks arising from the coexistence of alternating ZB and WZ InP segments in the same NW and (iv) the InP NW body. The occurrence and the characteristics of these PL features are correlated to the dominant crystal phase of the NWs, to the NW diameter and cross section as well as thickness and size of the confined materials. Most importantly, PL peaks centered at specific wavelength, with different relative intensities, linewidths and polarization behaviour can be achieved in the same individual nanowire in the energy range from 0.7 eV to 1.6 eV: this indicates that such multi-shell NWs can be used as multi-domain optically active polychromatic emitters. We performed numerical simulations of the electron and hole wavefunctions at different cross sections of the NWs, obtaining emission energies for the InAs island and QW in good agreement with the experimental results. We believe the present results are relevant in the frame of possible applications of InP-InAs-InP multi-shell nanowires in nanodevices for quantum information and communication technologies.

Acknowledgements

X. X. is supported by the National Natural Science Foundation of China under Grant No. 11721404, 51761145104, 61675228 and 11874419; the Strategic Priority Research Program of the Chinese Academy of Sciences under Grant No. XDB07030200 and XDB28000000, and CAS Interdisciplinary Innovation Team. A. L. is supported by the National Natural Science Foundation of China under Grant No. 51872008; We acknowledge financial support from the SUPERTOP project, QUANTERA ERA-NET Cofound in Quantum Technologies.

References

[1] Dasgupta N P, Sun J, Liu C, Brittman S, Andrews S C, Lim J, Gao H, Yan R and Yang P 2014 *Adv. Mater.* **26** 2137–2184
[2] Yeh C-Y, Lu Z W, Froyen S and Zunger A 1992 *Phys. Rev. B* **46** 10086
[3] De Luca M and Polimeni A 2017 *Applied Physics Reviews* **4** 041102
[4] Mishra A, Titova L V, Hoang T B, Jackson H E, Smith L M, Yarrison-Rice J M, Kim Y, Joyce H J, Gao Q, Tan H H and Jagadish C 2007 *Appl. Phys. Lett.* **91** 263104
[5] Arcangeli A, Rossella F, Tomadin A, Xu J, Ercolani D, Sorba L, Beltram F, Tredicucci A, Polini M and Roddaro S 2016 *Nano Lett.* **16** 5688-5693
[6] Niquet Y-M and Mojica D C 2008 *Phys. Rev. B* **77** 115316
[7] Zannier V, Rossi F, Dubrovskii V G, Ercolani D, Battiato S and Sorba L 2018 *Nano Lett.* **18** 167–174
[8] Heedt S, Wehrmann I, Weis K, Calarco R, Hardtdegen H, Grützmacher D, Schäpers Th, Morgan C and Bürgler D E 2013 Future Trends in Microelectronics: Frontiers and Innovations
[9] Poole P, Wu X, Lapointe J and Dalacu D 2016 *IEEE Photonics* Society Summer Topical Meeting Series (SUM) 195-196
[10] Bleszynski-Jayich A C, Fröberg L E, Björk M T, Trodahl H J, Samuelson L and Westervelt R M 2008 *Phys. Rev. B* **77** 245327
[11] Rossella F, Bertoni A, Ercolani D, Rontani M, Sorba L, Beltram F and Roddaro S 2014 *Nature Nanotechnology* **9** 997-1001
[12] Rossella F, Ercolani D, Sorba L, Beltram F and Roddaro S 2014 *J. Phys. D: Appl. Phys.* **47** 394015
[13] Reimer M E, Bulgarini G, Bakkers E P A M, Dalacu D, Poole P J and Zwiller V 2013 *Proceedings SPIE* **9** 861903
[14] Reimer M E, Bulgarini G, Akopian N, Hocevar M, Bouwes Bavinck M, Verheijen M A, Bakkers E P A M, Kouwenhoven L P and Zwiller V 2012 *Nat Commun* **3** 737
[15] Versteegh M A M, Reimer M E, Jöns K D, Dalacu D, Poole P J, Gulinatti A, Giudice A and Zwiller V 2014 *Nature Communications* **5** 5298
[16] Lindgren D, Kawaguchi K, Heurlin M, Borgstrom M T, Pistol M-E, Samuelson L and Gustafsson A 2013 *Nanotechnology* **24** 225203
[17] Alouane M H, Anufriev R, Chauvin N, Khmissi H, Naji K, Ilahi B, Maaref H, Patriarche G, Gendry M and Bru-Chevallier C 2011 *Nanotechnology* **22** 405702
[18] Masumoto Y, Goto K, Yoshida S, Sakuma Y, Mohan P, Motohisa J and Fukui T 2010 *Phys. Rev. B* **82** 075313
[19] Pal B, Goto K, Ikezawa M, Masumoto Y, Mohan P, Motohisa J and Fukui T 2008 *Appl. Phys. Lett.* **93** 073105
[20] Mohan P, Motohisa J and Fukui T 2006 *Appl. Phys. Lett.* **88** 133105
[21] Akopian N, Patriarche G, Liu L, Harmand J-C and Zwiller V 2010 *Nano Lett.* **10** 1198–1201
[22] Li A, Zou J and Han X 2016 *Sci China Mater* **59(1)** 51-91
[23] Buscemi F, Royo M, Bertoni A and Goldoni G 2015 *Phys. Rev. B* **92** 165302
[24] Buscemi F, Royo M, Goldoni G and Bertoni A 2016 *Nanotechnology* **27** 195201

Accepted Manuscript

[25] Zanolli Z, Pistol M-E, Fröberg L E and Samuelson L 2007 *J. Phys.:Cond. Matt.* **19** 295219
[26] Zanolli Z, Fuchs F, Furthmüller J, von Barth U and Bechstedt F 2007 *Phys. Rev. B* **75** 245121
[27] Fang Z M, Ma K Y, Jaw D H, Cohen R M, and Stringfellow G B, 1990 *Journal of Applied Physics* **67**, 7034
[28] Krishnamachari et al. 2004 *Appl. Phys. Lett.*, 85, 11
[29] Vu T T T, Zehender T, Verheijen M A, Plissard S R, Immink G W G, Haverkort J E M and Bakkers E P A M 2013 *Nanotechnology* **24** 115705
[30] Alouane M H H, Anufriev R, Chauvin N, Khmissi H, Naji K, Ilahi B, Maaref H, Patriarche G, Gendry M and Bru-Chevallier C 2011 *Nanotechnology* **22** 405702
[31] Loitsch B, Winnerl J, Grimaldi G, Wierzbowski J, Rudolph D, Morkötter S, Döblinger M, Abstreiter G, Koblmüller G and Finley J J 2015 *Nano Lett.* **15** 744-51
[32] Corfdir P, Van Hattem B, Uccelli E, Conesa-Boj S, Lefebvre P, Fontcuberta i Morral A and Phillips R T 2013 *Nano Lett.* **13** 5303−5310
[33] Sitek A, Torres M U, Torfason K, Gudmundsson V, Bertoni A and Manolescu A 2018 *Nano Lett.* **18** 2581
[34] Seguin R, Schliwa A, Rodt S, Pötschke K, Pohl U W and Bimberg D 2005 *Phys. Rev. Lett.* **95** 257402
[35] Bouwmeester D, Ekert A K and Zeilinger A 2000 The physics of quantum information, Springer, Berlin
[36] Stevenson R M, Young R J, Atkinson P, Cooper K, Ritchie D A and Shields A J 2006 *Nature* **439** 179
[37] Xu X, Williams D A and Cleaver J R A 2005 *Appl. Phys. Lett.* **86** 012103
[38] Qian C, Wu S, Song F, Peng K, Xie X, Yang J, Xiao S, Steer M J, Thayne I G, Tang C, Zuo Z, Jin K, Gu C and Xu X 2018 *Phys. Rev. Lett.* **120** 213901
[39] Bayer M, Ortner G, Stern O, Kuther A, Gorbunov A A, Forchel A, Hawrylak P, Fafard S, Hinzer K, Reinecke T L, Walck S N, Reithmaier J P, Klopf F and Schäfer F 2002 *Phys. Rev. B* **65** 195315

Accepted Manuscript